

University of Groningen

Enhancing the Potential of Fused Heterocycle-Based Triarylhydrazone Photoswitches

Hegedüsová, Lea; Blaise, Nadine; Pašteka, Lukáš F.; Budzák, Šimon; Medved', Miroslav; Filo, Juraj; Mravec, Bernard; Slavov, Chavdar; Wachtveitl, Josef; Grabarz, Anna M.

Published in:
Chemistry - A European Journal

DOI:
[10.1002/chem.202303509](https://doi.org/10.1002/chem.202303509)

IMPORTANT NOTE: You are advised to consult the publisher's version (publisher's PDF) if you wish to cite from it. Please check the document version below.

Document Version
Publisher's PDF, also known as Version of record

Publication date:
2024

[Link to publication in University of Groningen/UMCG research database](#)

Citation for published version (APA):

Hegedüsová, L., Blaise, N., Pašteka, L. F., Budzák, Š., Medved', M., Filo, J., Mravec, B., Slavov, C., Wachtveitl, J., Grabarz, A. M., & Cigáň, M. (2024). Enhancing the Potential of Fused Heterocycle-Based Triarylhydrazone Photoswitches. *Chemistry - A European Journal*, 30(8), Article e202303509. <https://doi.org/10.1002/chem.202303509>

Copyright


Other than for strictly personal use, it is not permitted to download or to forward/distribute the text or part of it without the consent of the author(s) and/or copyright holder(s), unless the work is under an open content license (like Creative Commons).

The publication may also be distributed here under the terms of Article 25fa of the Dutch Copyright Act, indicated by the "Taverne" license. More information can be found on the University of Groningen website: <https://www.rug.nl/library/open-access/self-archiving-pure/taverne-amendment>.

Take-down policy

If you believe that this document breaches copyright please contact us providing details, and we will remove access to the work immediately and investigate your claim.

Downloaded from the University of Groningen/UMCG research database (Pure): <http://www.rug.nl/research/portal>. For technical reasons the number of authors shown on this cover page is limited to 10 maximum.

 Hot Paper


Enhancing the Potential of Fused Heterocycle-Based Triarylhydrazone Photoswitches

Lea Hegedüsová,^[a] Nadine Blaise,^[b] Lukáš F. Pašteka,^[c, d] Šimon Budzák,^[e] Miroslav Medved',^[e, f] Juraj Filo,^[a] Bernard Mravec,^[a] Chavdar Slavov,^[g] Josef Wachtveitl,^[b] Anna M. Grabarz,^{*,[d, h]} and Marek Cigán',^{*,[a]}

Triarylhydrazones represent an attractive class of photochromic compounds offering many interesting features including high molar absorptivity, good addressability, and extraordinary thermal stability. In addition, unlike most other hydrazone-based photoswitches, they effectively absorb light above 365 nm. However, previously prepared triarylhydrazones suffer from low quantum yields of the $Z \rightarrow E$ photoisomerization. Here, we have designed a new subclass of naphthoyl-benzothiazole hydrazones that balance the most beneficial features of

previously reported naphthoyl-quinoline and benzoyl-pyridine triarylhydrazones. These preserve the attractive absorption characteristics, exhibit higher thermal stability of the metastable form than the former and enhance the rate of the $Z \rightarrow E$ photoisomerization compared to the later, as a result of the weakening of the intramolecular hydrogen bonding between the hydrazone hydrogen and the benzothiazole moiety. Introducing the benzothiazole motif extends the tunability of the photochromic behaviour of hydrazone-based switches.

Introduction

Over the past years, advanced molecular materials capable of changing their physicochemical properties under external stimulus have been attracting growing scientific interest.^[1–8] The most attractive representatives of the stimuli-responsive compounds are certainly photoswitches,^[9–12] exhibiting a photo-induced reversible structural transformation between stable and metastable forms. Owing to this property, they were adapted to numerous applications, including optoelectronics,^[13,14] solar energy storage,^[15–17] photopharmacology,^[18–23] and photo-controlled drug delivery.^[24]

Various structural motifs leading to the photochromic behavior have been identified in the past (e.g., diarylethenes, azobenzenes, spiropyrans, hemithioindigos, and iminothioindoxyls) offering a large palette of compounds with diverse properties tunable for a particular application. An important class complementing attractive features of other photoswitches involves hydrazones which exhibit bistable photoswitching stemming from exceptionally high thermal stability of the metastable isomer, fast photoisomerization, resistance to hydrolysis, straightforward synthesis, and easy skeleton modularity.^[25,26] First photo-active hydrazones were already reported by Kuhn in 1952^[27] and later by Pichon and Courtot in 1980s.^[28] However, their great photochromic potential remained hidden until 2017 when Aprahamian and his co-workers developed new diarylhydrazone photoswitches^[29,30] which found their use in many applications. These include reversible glass transition temperature photomodulation and hardening of polymers,^[31] photoremovable templates for cost effective and environmentally friendly γ -cyclodextrin isolation,^[32] photoregulated drug release using an emissive ketoester hydrazone photoswitch-modified copolymer,^[24] and solar thermal energy storage in strained cyclic ketoester hydrazones.^[16] Diarylhydrazones/diarylacylhydrazones were also studied by Lehn's^[33] and

[a] L. Hegedüsová, J. Filo, B. Mravec, M. Cigán'
 Department of Organic Chemistry,
 Faculty of Natural Sciences, Comenius University
 Bratislava, 84215 (Slovakia)
 E-mail: marek.cigan@uniba.sk

[b] N. Blaise, J. Wachtveitl
 Institute of Physical and Theoretical Chemistry, Faculty of Biochemistry,
 Chemistry, Pharmacy, Goethe University
 Frankfurt am Main, 60438 (Germany)

[c] L. F. Pašteka
 Van Swinderen Institute for Particle Physics and Gravity,
 University of Groningen
 Groningen, 9747AG (The Netherlands)

[d] L. F. Pašteka, A. M. Grabarz
 Department of Physical and Theoretical Chemistry,
 Faculty of Natural Sciences, Comenius University
 Bratislava, 84215 (Slovakia)
 E-mail: anna.grabarz@pwr.edu.pl

[e] Š. Budzák, M. Medved'
 Department of Chemistry, Faculty of Natural Sciences,
 Matej Bel University
 Banská Bystrica, 97400 (Slovakia)

[f] M. Medved'
 Regional Centre of Advanced Technologies and Materials,
 Czech Advanced Technology and Research Institute,
 Palacký University Olomouc
 Olomouc, 77900 (Czechia)

[g] C. Slavov
 Department of Chemistry, University of South Florida
 Tampa, FL 33620, Florida (US)

[h] A. M. Grabarz
 Institute of Advanced Materials, Faculty of Chemistry,
 Wrocław University of Science and Technology
 Wrocław, 50370 (Poland)

Supporting information for this article is available on the WWW under
<https://doi.org/10.1002/chem.202303509>

Hecht's groups^[34] showing high substitutional tunability of thermal stability and optical properties as well as their potential for designing multiple state molecular devices.

Recently, our group reported the photochromic behaviour of triarylhydrazones, thus completing the mosaic of hydrazone-based photoswitches.^[35,36] Compared to previous hydrazone-based photoswitches, the designed triarylhydrazones containing a pyridine/quinoline acceptor in the ketone part featured higher extinction coefficients, better separation of absorption maxima, and lower, but yet still attractive thermal stability that was found to be less sensitive to electron-donor substitution. Importantly, they also exhibited an effective absorption maximum red-shift of both isomers above 365 nm. However, most of the investigated triarylhydrazones displayed $Z \rightarrow E$ quantum yields (QYs) below 1%.

Mechanistically, the low $Z \rightarrow E$ photoisomerization QYs were attributed to two competitive non-radiative pathways. First, the S_1 state of the Z isomer is stabilized by an intramolecular hydrogen bond between the hydrazone hydrogen and heterocycle nitrogen atoms. Second, in the case of quinoline hydrazones, excited-state intramolecular proton transfer (ESIPT) from the $-NH$ group to the heterocycle initiates non-radiative

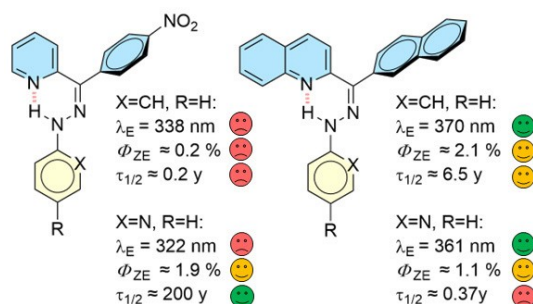
deactivation of the excited state hampering the isomerization. Our computations also revealed that N -inversion is the rate-determining step in a complex sequential mechanism of thermal $E \rightarrow Z$ isomerization and the activation barrier can be tuned by introducing suitable electron donating/withdrawing substituents in the hydrazine part (see Figure 1). Furthermore, we showed that the red-shift of absorption maxima achieved by the planarization of Aprahamian's ketoester hydrazones,^[37] which was however accompanied with an undesirable acceleration of the back thermal reaction, can also be realized via extending the π -conjugation in triarylhydrazones bearing fused aromatic rings without a dramatic drop of their thermal stability. Structurally, triarylhydrazones offer ample room for the optimization of photochromic properties by (i) combining aryls with different electron donor/acceptor capacity, (ii) controlling the strength of the intramolecular H-bond (both in the ground or excited states), and/or (iii) altering the extent of π -conjugation. Clearly, balanced optimization of all pertinent features remains a challenging task requiring smart design strategies based on detailed mechanistic insights from computations.

Results and Discussion

Herein, we present a series of five new naphthoyl-benzothiazole hydrazones diversified by the p -phenyl substituent (Figure 1 and Scheme 1, ordered according to the increasing electron-withdrawing character of the substituent). In designing this series, we aimed at (i) increasing the QY of $Z \rightarrow E$ photoisomerization of previously prepared triarylhydrazones, (ii) enhancing thermal stability compared to naphthoyl-quinoline triarylhydrazones, while (iii) maintaining (or improving) their good addressability and the advantageous red-shift of the E isomer's absorption maximum to the region above 365 nm.

The replacement of pyridine/quinoline by a benzothiazole unit was expected beneficial for facilitating the $Z \rightarrow E$ photoisomerization due to weakening the intramolecular H-bond in the excited state of the Z isomer. In addition, a slowdown of the thermal $E \rightarrow Z$ back-reaction was anticipated, since the inversion transition state structure would be destabilized by repulsion between lone pairs of imine nitrogen and the thiazole heteroatoms. To keep the absorption maxima of E isomer red-shifted, naphthyl was exclusively used in the ketone moiety. Finally, various electron withdrawing/donating groups were introduced into the hydrazine part to pursue a possibility of fine-tuning the photochromic properties of the proposed

Mravec et al., 2021



This work:

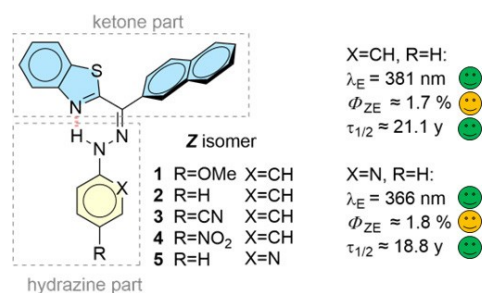
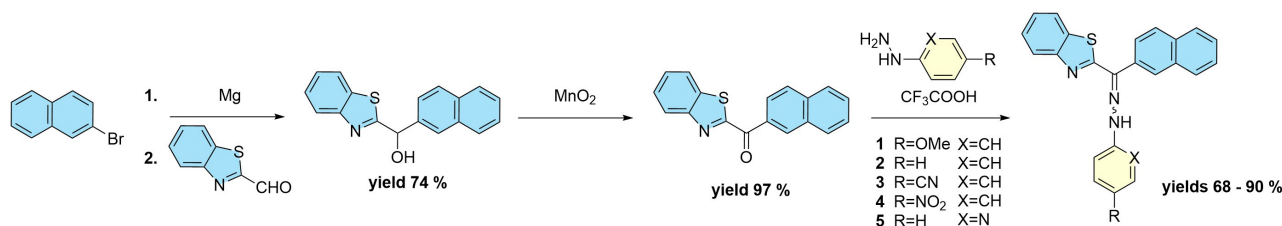


Figure 1. Molecular structure of known triarylhydrazone photoswitches.



Scheme 1. Brief synthetic route of the studied hydrazones.

hydrazone skeleton (for details of synthesis, see Section 1.4 in the Supporting Information).

Experimental determination of fundamental photoswitching parameters of all designed hydrazones was followed by a more detailed investigation of the photo-isomerizations of the parent compound **2** by means of ultrafast transient absorption (TA) spectroscopy. The measurements confirmed an increase of thermal stability of the *E* form as well as an acceleration of the ES dynamics with regard to previous triarylhydrazones, while the rates of the *Z*→*E* photoisomerization were found comparable to the most efficient quinoline derivative.

To rationalize the main features of new compounds, (time-dependent) density functional theory (TD)-DFT calculations were performed addressing the optical properties of *Z* and *E* isomers, kinetic stability of meta-stable forms, and reaction mechanisms of thermal isomerizations, including the analysis of substituent and solvent effects. Detailed information concerning computational protocol can be found in the Supporting Information (Section 5.1). Experimental spectroscopic parameters for both *Z* and *E* forms of all studied compounds were compared with those computed using several universally high-performing exchange-correlation functionals (CAM-B3LYP, M06-2X, and MN15) in combination with the def2-TZVPP basis set

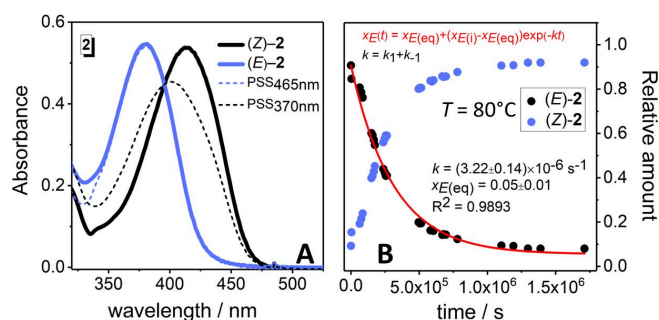


Figure 2. Photochromic behaviour of hydrazone **2** in toluene (left; PSS_x – Photostationary State at irradiation wavelength X) and kinetics of thermal *E*→*Z* isomerization of thermodynamically less stable *E* isomer measured at 80 °C (right; x_E denotes relative amount of the *E* isomer, k_1 and k_{-1} are rate constants for thermal *E*→*Z* and *E*→*E* isomerizations, respectively).

(Figure S45 and Table S3). Based on this comparison, MN15 was selected for the systematic analysis of electronic transitions as well as the inspection of thermal reaction energies and activation barriers.

Figure 2 shows the bistable P-type photoswitching character of prepared triarylhydrazones, with light-induced *E*→*Z* (370 nm) and *Z*→*E* (465 nm) photoisomerizations, confirming a good addressability (Figure 2A) and high thermal stability even at elevated temperature (Figure 2B). Importantly, the half-lives of thermodynamically less stable *E* isomers range from 15 to 157 years at room temperature (Table 1) and thus are ca. 2–24 times larger than the half-life of the most promising 2-(naphthoyl)quinoline analogue equal to 6.5 years.

Interestingly, the thermal stability of benzothiazole triarylhydrazones is less dependent on the *p*-phenyl substitution compared to the previously studied pyridine and quinoline derivatives.^[36] Owing to a weakened intramolecular H-bond in the *Z* isomer, the thermodynamic stability of *Z* and *E* forms becomes comparable ($\Delta_r G \geq -2$ kcal/mol). This is confirmed by DFT calculations which predict the $\Delta_r G$ values in agreement with experiment (Table S8). Consequently, the rate constants for *E*→*Z* and *Z*→*E* thermal isomerizations are within one order of magnitude. It is worth noting that in the case of pyridine and quinoline derivatives the thermal *Z*→*E* isomerization was not observed at all or, in some cases, only as a two-orders-of-magnitude less favorable process. On the other hand, K_{eq} for compound **5** equals 3.3 (Table 1). This corroborates the role of hydrogen bonding in *Z* isomers, which is the strongest in pyridine ($pK_a = 5.2$) followed by quinoline ($pK_a = 4.9$), and the weakest in benzothiazole ($pK_a = 1.7$).

Notably, DFT calculations revealed that the benzothiazole moiety in the most stable *E* conformers is rotated by 180° w.r.t. the global minimum structure of *Z* (see Figure S37). This was attributed to weaker repulsion between lone pairs of imine nitrogen and sulphur atoms compared to benzothiazole nitrogen-imine nitrogen repulsion (cf. Mulliken atomic charges in Figure S44).

The thermal *E*→*Z* isomerization proceeds via an inversion mechanism similarly to pyridine derivatives.^[36] However, in the

Table 1. Thermal stability of hydrazones 1–5 in toluene at 25 °C.

Der.		k [10 ⁻¹⁰ s ⁻¹]	$\tau_{1/2}$ [years]	ΔG^\ddagger [kcal/mol]	$\Delta_r G$ [kcal/mol]	K_{eq} [<i>Z</i> / <i>E</i>]
1	<i>E</i> → <i>Z</i>	14.73(17)	14.9(17)	29.50(7)	-1.53(14)	13.1(32)
	<i>Z</i> → <i>E</i>	1.12(24)	196(42)	31.03(12)		
2	<i>E</i> → <i>Z</i>	10.42(11)	21.1(22)	29.71(6)	-2.00(18)	29.0(90)
	<i>Z</i> → <i>E</i>	0.36(11)	612(180)	31.70(17)		
3	<i>E</i> → <i>Z</i>	1.40(17)	157(19)	30.90(7)	-1.66(21)	16.4(58)
	<i>Z</i> → <i>E</i>	0.09(3)	2585(856)	32.55(20)		
4	<i>E</i> → <i>Z</i>	2.93(28)	75(8)	30.46(6)	-1.11(10)	6.5(10)
	<i>Z</i> → <i>E</i>	0.45(6)	488(63)	31.57(8)		
5	<i>E</i> → <i>Z</i>	11.65(11)	18.8(17)	29.64(5)	-0.70(8)	3.3(4)
	<i>Z</i> → <i>E</i>	3.57(34)	62(58)	30.34(6)		

Italic font indicates parameters associated with parent compound **2**.

case of benzothiazole analogues the inversion as the rate-limiting step is preceded by formation of a relatively stable sandwich-type E_{conf} conformer (TS_E barrier 13.5 kcal/mol). This structure is stabilized by π - π stacking interactions between the hydrazine phenyl (N–N single bond rotation) and ketone naphthalene rings (Figure 3). Notably, a similar sandwich-like structure (referred to as L_1 in Ref. [35]) appears as a metastable Z conformer after initial inversion in pyridines. In turn, the benzothiazole inversion through the activation barrier of 21.4 kcal/mol (TS_{inv}) advances to a local minimum Z_{conf} featuring an arrangement similar to a metastable Z conformer in pyridines (L_2 in Ref. [35]). The last step involves a less energy-demanding mutual rotation of condensed aromatic rings (TS_Z) and leads to the optimal Z isomer configuration.

The activation Gibbs energy slightly decreases with the increasing solvent polarity (e.g., $\Delta G_{E \rightarrow Z}^\ddagger = 29.71$ and 28.09 kcal/mol for **2** in toluene and acetonitrile, respectively; see Table 1 and Table S2). The observed decline is qualitatively reproduced by DFT calculations (the corresponding values are 29.86 and 27.91 kcal/mol, respectively). Let us note that the small differences between the $E \rightarrow Z$ barriers (< 1 kcal/mol) for the systems studied here are below the accuracy threshold of DFT for

activation barriers,^[38,39] and therefore the observed subtle substitutional effects cannot be rationalized by the applied methodology (Figure S38 see Supporting Information).

Although the replacement of quinoline with benzothiazole slightly worsens the separation of absorption maxima compared to quinoline derivatives, it simultaneously increases the Z isomer's molar absorption coefficient and favors the $Z \rightarrow E$ photoisomerization even in protic methanol (Figure S41). Interestingly, introducing either strong electron-donating or electron-withdrawing (ED or EW) substituents in the p -phenyl position (compounds **1** and **4**) causes a red-shift of absorption maxima, and the substitution has practically no effect on the band separation. Both observations are in line with our TD-DFT calculations (Table 2). The observed red-shift of λ_{max} for both isomers of hydrazones **1** and **4** can be explained by a smaller HOMO–LUMO gap caused by (i) an increase in the HOMO energy due to the presence of a strong ED methoxy substituent and (ii) a significant decrease in the LUMO energy in the case of the strongest EW nitro group, for **1** and **4** respectively (see Table 3, Table S4 and Figure S43).

The TD-DFT analysis also revealed that the absorption bands of both Z and E isomers observed above 365 nm correspond to the S_0 – S_1 transition which can be described as a $\pi \rightarrow \pi^*$

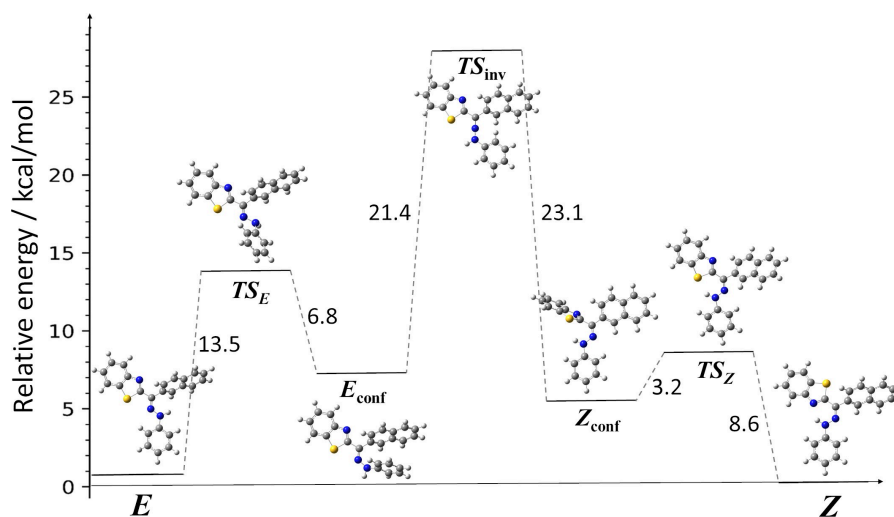


Figure 3. Reaction path profile for thermal E - Z transformation of hydrazone **2** calculated MN15/def2-TZVPP level of theory.

Table 2. Experimental and computed absorption maxima (in nm), the band separation ($\Delta\lambda_{\text{max}}(Z-E)$) and related oscillator strengths (f) corresponding to the lowest lying ($\pi \rightarrow \pi^*$) transitions in toluene. Theoretical data were determined using vertical approximation at the MN15/def2-TZVPP level of theory.

Der.	Calc.					Exp.				
	λ_{max}	f	λ_{max}	f	$\Delta\lambda_{\text{max}}$	λ_{max}	f	λ_{max}	f	$\Delta\lambda_{\text{max}}$
1	399	0.77	381	0.74	18	429	0.48	394	0.47	35
2	379	0.73	362	0.73	17	415	0.42	381	0.48	34
3	376	0.93	358	0.97	18	410	0.57	379	0.51	31
4	384	1.04	369	1.10	15	433	0.89	398	0.68	35
5	363	0.74	348	0.74	15	392	0.42	366	0.51	26

Italic font indicates parameters associated with parent compound **2**.

Table 3. Photoswitching parameters of hydrazones measured in toluene.

Der.	ϵ [L/(mol·cm)]		λ_{\max} [nm]		$\Phi_{E \rightarrow Z}$ [%]	$\Phi_{Z \rightarrow E}$ [%]	$PSS_{E \rightarrow Z}$ (E/Z)	$PSS_{Z \rightarrow E}$ (E/Z)
	<i>E</i>	<i>Z</i>	<i>E</i>	<i>Z</i>				
1	23400	24429	394	429	1.7(2)	1.5(1)	26:74	96:4
2	27600	26875	381	415	2.3(2)	1.7(3)	24:76	96:4
3	29100	34494	379	410	4.1(5)	0.21(3)	16:84	98:2
4	35300	37695	398	433	10.5(12)	1.1(4)	4:96	75:25
5	28400	28008	366	392	3.3(1)	1.80(3)	27:73	74:26

Italic font indicates parameters associated with parent compound 2.

excitation occurring predominantly from HOMO to LUMO (see Table S4). Electron density difference (EDD) plots for both *E* and *Z* forms (independently on a substituent) indicate that the excitation is accompanied with a strong charge transfer (CT) from the phenyl and NH groups to a π^* orbital mostly localized along the C(btz)–C bond and spreading towards the benzothiazole moiety (see Tables S5–S6). The CT character is significantly affected by the nature of a *p*-phenyl substituent. Whereas the ED methoxy substituent in 1 promotes the charge transfer, the EW groups in 3–5 act in the opposite way.

Notably, the naphthyl moiety is only marginally involved in the $S_0 \rightarrow S_1$ excitation, which is due to its distortion from the main molecular plane, and its role depends on the isomer. Whereas in *E* isomers (except (*E*-4)) it behaves as a secondary acceptor, in *Z* forms it acts as secondary donor.

The observed red-shift of the absorption maxima *between* the *Z* and *E* forms can be explained by a more efficient involvement of the benzothiazole nitrogen's *p* orbital and partially also the benzene part of benzothiazole into the π -conjugated system facilitated by the intramolecular H-bond present in the *Z* isomer (see EDD plots in Table S5). The investigated transitions are associated with moderate to high computed oscillator strengths (within 0.7–1.2 range). Although being systematically larger, calculated oscillator strengths closely follow the trends observed experimentally (see Table 2 and Figure S42). The differences in *f* values between individual derivatives reflect the CT character of the transitions – the smaller the CT distance (d_{CT}) value,^[40,41] the larger the overlap of initial and final states, and thus the larger *f*. It is also worth noting that some of the observed absorption bands (e.g., in the case of 4) feature deviations from a symmetric shape, which are associated with the vibrational progression as revealed by calculations of the corresponding vibronic spectra (Figure 4 and Figure S46).

Photochemical efficiency of *E*→*Z* photoisomerization resembles the efficiency observed in other triarylhydrazones,^[35,36,42] with QYs spanning across a wide range of 1.7–10.5% (Table 3). Furthermore, similarly to the previously studied pyridine and quinoline derivatives, the QYs of the *Z*→*E* photo-transformation are much lower (1.1–1.8%). Although these QYs are slightly lower than those of the most efficient naphthylquinolines (with QYs=2.0–2.1%),^[36] the photoconversion rates for these two

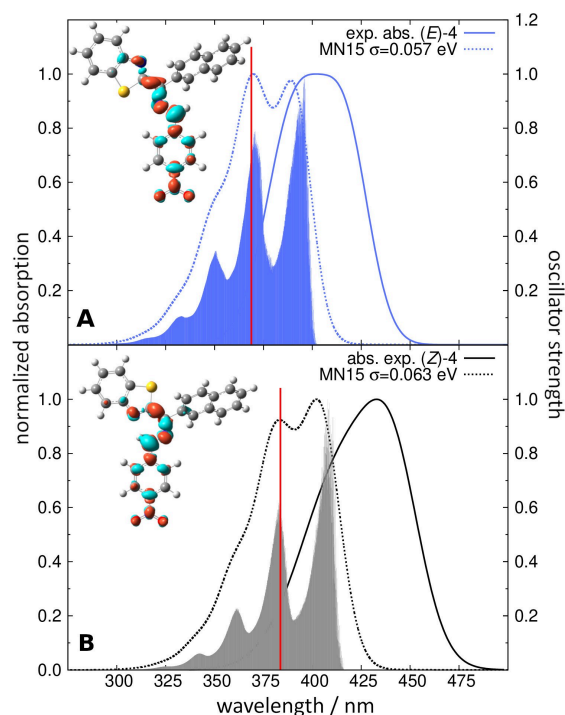


Figure 4. Spectral simulations of the *E* (A) and *Z* isomers (B) of 4 were performed employing the IMDHO approach^[43,44] at the MN15/def2-TZVPP theory level. The non-homogeneous broadening parameters (σ) are given in the legend. Inset EDD plots were simulated using 0.002 a.u. contour value.

types of triarylhydrazones are similar because of higher molar absorption coefficients in the case of benzothiazole hydrazones. Let us note that much higher rates were reported for ketoester diaryhydrazones.^[30]

The dynamics of the photoinduced transformation of the prepared hydrazones was studied by ultrafast spectroscopy (see Refs. [45,46] for set-up and data analysis details). The *E*→*Z* photoisomerization of parent hydrazone 2 in *n*-hexane was triggered by direct excitation of the (*E*-2) using ultrashort (ca. 100 fs) laser pulses centered at 365 nm. The transient data (Figure 5A) are dominated by four components – two excited state absorption (ESA) bands, a narrow positive signature at long delay times accounting for the formation of the photo-product (*Z*-2), and a negative ground state bleach (GSB) band. Abandoning the Franck–Condon geometry, reflected by an

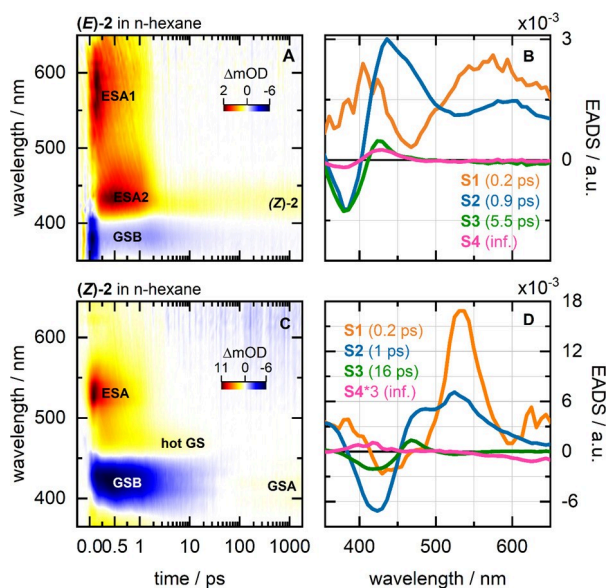


Figure 5. Transient absorption data and corresponding evolution-associated difference spectra (EADS) of (*E*)-2 upon excitation at 365 nm (A,B), and of (*Z*)-2 upon excitation at 420 nm (C,D) in n-hexane. The color coding of the transient absorption data is as follows: i) light to dark blue – negative absorption difference signal corresponding to ground state bleach; ii) yellow through red to black – positive absorption difference signal corresponding to excited-state, hot ground-state, and photoproduct absorption. During the ultrafast experiments, to prevent photoproduct accumulation and maintain stationary states dominated by the *E*- or by the *Z*-isomer, the samples were continuously irradiated with a 455 nm or with a 365 nm LED.

ultrafast decay (200 fs lifetime) of the initial broad ESA1 band (550 nm), leads to a concomitant rise of ESA2 (450 nm, 900 fs lifetime). The ESA2 band extending to the blue spectral region significantly overlaps with the GSB band and thus effectively reduces the negative difference absorption in this spectral region (ca. 370 nm; see Figure 5B, signature S2).

The depopulation of the excited state of (*E*)-2 manifested by the decay of the ESA2 band is accompanied with the formation of a positive absorption signature (400–450 nm), which can be ascribed predominantly to (*E*)-2 hot GS absorption. The hot GS undergoes vibrational cooling with ca. 5.5 ps lifetime (Figure 5B, signature S3) and reveals the remaining positive absorption difference band at ca. 425 nm, as described by the S4 spectrum (Figure 5B, signature S4). The latter accounts for the formation of the photoproduct (*Z*)-2. Similar dynamics was observed in acetonitrile, which however shows a more distributed excited state decay dynamics and slower vibrational relaxation in the GS (Figure S30D, signature S5).

The *Z*→*E* excited-state dynamics of (*Z*)-2 in n-hexane was selectively initiated using ultrashort pulses centered at 420 nm. The transient data (Figure 5C) show a dual band (370 nm and 530 nm) ESA signature which overlaps with the negative GSB band (400–470 nm). The 370 nm and 530 nm ESA bands undergo ultrafast decay (ca. 200 fs lifetime, Figure 5D, signature S1) accompanied by the growth of a weaker positive band at 490 nm (Figure 5D, signature S2). The decay of the latter band, and thus of the ES (ca. 1 ps) leads to the recovery of the GSB (420 nm) and to the formation of a narrower positive hot GS

signature at 480 nm. The hot (*Z*)-2 GS cools down with a 16 ps lifetime. The overall dynamic is slightly slower in acetonitrile (see Figures S30–S31). Notably, in both solvents the cooling reveals a weak positive absorption (Figure 5C GSA, described by signature S4 in Figure 5D) overlapping with the (*Z*)-2 GSB.

This signature could be assigned to a combination of an alternative, high energy ground-state intramolecular proton transfer (GSIPT) population, which decays on the microsecond time scale as indicated by our flash photolysis expedients (Figure S32), and a less intense GS absorption of the photoproduct (*E*)-2 at approximately 380 nm due to relatively low *Z*→*E* photoisomerization efficiency (see Supporting Information page S-42).

In analogy with triarylhydrazones,^[35] no stable structure was found (at the TD-DFT level) on the excited state surface of the *E* isomer (Figure 6), meaning that barrier-less transformation toward conical intersection (CI) takes place. This is reflected in higher QYs of the *E*→*Z* photoisomerization compared to *Z*→*E*. Nevertheless, the highest QYs of the *E*→*Z* are 10.5% hinting to unfavourable branching ratio (*E* to *Z*) of the corresponding CI.

In the *Z* isomer we have found local minima on the ES potential energy surface. Contrary to previously studied hydrazones, the molecule remained quasi-planar with the dihedral angle Ar(C)–N–N=C being equal to 174°. Such a structure is well separated from the GS surface with estimated emission wavelength of 485 nm for **2**. According to relaxed scans, this minimum is protected by negligible barrier of <1 kcal/mol from C=N rotation. ESIPT process is kinetically feasible (the barrier is ~3 kcal/mol) and is coupled with N–N rotation ending in the CI without *Z*→*E* isomerization. Only first of the mentioned processes can lead to *E* isomer, which explains the low *Z*→*E* QY.

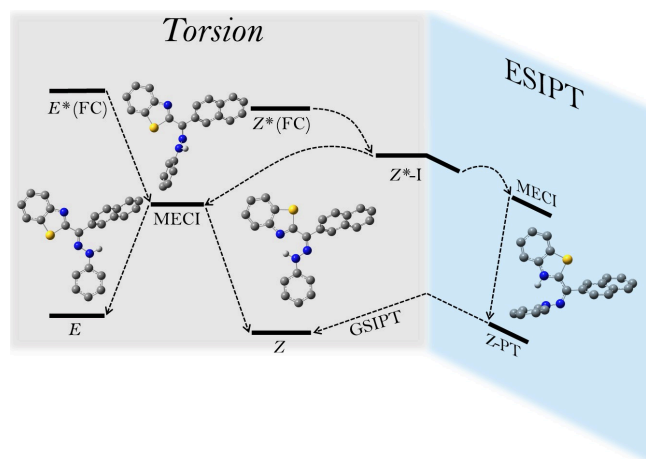


Figure 6. Possible de-excitation paths for **2** calculated at MN15/def2-TZVP (stable forms) and Mixed Reference Spin-Flip (MSRF)^[47,48] TD-BHLLYP/6-31G(d) (MECI) levels of theory. Hydrogens uninvolved in the de-excitation were hidden to clear up the view.

Conclusion

We demonstrated that the incorporation of a benzothiazole unit allowed the red-shift of absorption bands of both isomers to a more desirable spectral range above 365 nm and simultaneously stabilized the thermodynamically less stable form with respect to the previously most promising 2-(naphthoyl)quinoline triarylhydrazone photoswitch. Another benefit of this modification is the weakening of the *Z* isomer intramolecular hydrogen bonding in the first excited state, leading to enhanced rate of *Z*→*E* photoisomerization compared to benzoyl-pyridine analogues. Last, but not least, the replacement of pyridine with the benzothiazole motive extends the possibilities of the skeleton modification, which opens a route to the synthesis of highly tunable triarylhydrazones functionalized on all three aromatic rings.

Supporting Information

Raw NMR data are available from the authors on request. The authors have cited additional references within the Supporting Information.^[49–64]

Acknowledgements

Financial support of the Slovak Research and Development Agency (APVV-20-0098) is acknowledged. C.S. and J.W. acknowledge Deutsche Forschungsgemeinschaft (WA 1850/4-3). B.M., J.F., L.H. and M.C. acknowledge the support from the Operation Program of Integrated Infrastructure for the project: Advancing University Capacity and Competence in Research, Development and Innovation, ITMS2014+: 313021X329, co-financed by the European Regional Development Fund. L. F. P. acknowledges the support from the Dutch Research Council (NWO) project number VI.C.212.016 of the talent programme VICI. This research used generous resources of a Wrocław Supercomputer and Networking Center and High Performance Computing Center of Matej Bel University in Banská Bystrica using the HPC infrastructure acquired in projects ITMS 26230120002 and 26210120002 (Slovak infrastructure for high performance computing) supported by the Research and Development Operational Program funded by the ERDF.

Conflict of Interests

There are no conflicts to declare.

Data Availability Statement

The data that support the findings of this study are available from the corresponding author upon reasonable request.

Keywords: hydrazones · photoswitches · TD-DFT · thermal stability · transient absorption

- [1] M. Su, Y. Song, *Chem. Rev.* **2022**, *122*, 5144–5164.
- [2] R. E. Newnham, *MRS Bull.* **1997**, *22*, 20–34.
- [3] R. M. El-Shishtawy, *Int. J. Photoenergy* **2009**, *2009*, 21.
- [4] S. Vigneshvar, B. Senthikumar, *Med. Devices Sens.* **2018**, *1*, e10011.
- [5] H. Wang, H. K. Bisoyi, X. Zhang, F. Hassan, Q. Li, *Chem. Eur. J.* **2022**, *28*, e202281861.
- [6] C. P. Collier, E. W. Wong, M. Belohradský, F. M. Raymo, J. F. Stoddart, P. J. Kuekes, R. S. Williams, J. R. Heath, *Science* **1999**, *285*, 391–394.
- [7] S. Erbas-Cakmak, S. Kolemen, A. C. Sedgwick, T. Gunnlaugsson, T. D. James, J. Yoon, E. U. Akkaya, *Chem. Soc. Rev.* **2018**, *47*, 2228–2248.
- [8] S. Mucicoy, M. I. Álvarez Echazú, P. E. Antezana, J. M. Galdopórpura, C. Olivetti, A. M. Mebert, M. L. Foglia, M. V. Tuttolomondo, G. S. Alvarez, J. G. Hardy, M. F. Desimone, *Int. J. Mol. Sci.* **2020**, *21*, 4724.
- [9] M.-M. Russew, S. Hecht, *Adv. Mater.* **2010**, *22*, 3348–3360.
- [10] J. Boelke, S. Hecht, *Adv. Opt. Mater.* **2019**, *7*, 1900404.
- [11] K. Matsuda, M. Irie, *J. Photochem. Photobiol.* **2004**, *5*, 169–182.
- [12] A. Goulet-Hanssens, F. Eisenreich, S. Hecht, *Adv. Mater.* **2020**, *32*, 1905966.
- [13] E. Orgiu, P. Samorì, *Adv. Mater.* **2014**, *26*, 1827–1845.
- [14] L. Hou, X. Zhang, G. F. Cotella, G. Carnicella, M. Herder, B. M. Schmidt, M. Pätzl, S. Hecht, F. Cacialli, P. Samorì, *Nat. Nanotechnol.* **2019**, *14*, 347–353.
- [15] C.-L. Sun, C. Wang, R. Boulatov, *ChemPhotoChem* **2019**, *3*, 268–283.
- [16] Q. Qiu, S. Yang, M. A. Gerkman, H. Fu, I. Aprahamian, G. G. D. Han, *J. Am. Chem. Soc.* **2022**, *144*, 12627–12631.
- [17] A. U. Petersen, Z. Wang, P. Erhart, M. B. Nielsen, K. Moth-Poulsen, *Nat. Commun.* **2018**, *9*, 1945.
- [18] W. A. Velema, W. Szymanski, B. L. Feringa, *J. Am. Chem. Soc.* **2014**, *136*, 2178–2191.
- [19] M. J. Fuchter, *J. Med. Chem.* **2020**, *63*, 11436–11447.
- [20] J. Broichhagen, J. A. Frank, D. Trauner, *Acc. Chem. Res.* **2015**, *48*, 1947–1960.
- [21] M. M. Lerch, M. J. Hansen, G. M. van Dam, W. Szymanski, B. L. Feringa, *Angew. Chem. Int. Ed.* **2016**, *55*, 10978–10999.
- [22] M. Jeong, J. Park, Y. Seo, K. Lee, S. Pramanik, S. Ahn, S. Kwon, *Chem. Eur. J.* **2022**, *28*, e202103972.
- [23] M. Zhu, H. Zhou, *Org. Biomol. Chem.* **2018**, *16*, 8434–8445.
- [24] X. Guo, B. Shao, S. Zhou, I. Aprahamian, Z. Chen, *Chem. Sci.* **2020**, *11*, 3016–3021.
- [25] X. Su, I. Aprahamian, *Chem. Soc. Rev.* **2014**, *43*, 1963–1981.
- [26] J. D. Harris, M. J. Moran, I. Aprahamian, *Proc. Nat. Acad. Sci.* **2018**, *115*, 9414–9422.
- [27] R. Kuhn, W. Münzing, *Chem. Ber.* **1952**, *85*, 29–37.
- [28] R. Pichon, J. Le Saint, P. Courtot, *Tetrahedron* **1981**, *37*, 1517–1524.
- [29] H. Qian, S. Pramanik, I. Aprahamian, *J. Am. Chem. Soc.* **2017**, *139*, 9140–9143.
- [30] B. Shao, H. Qian, Q. Li, I. Aprahamian, *J. Am. Chem. Soc.* **2019**, *141*, 8364–8371.
- [31] S. Yang, J. D. Harris, A. Lambai, L. L. Jeliakzov, G. Mohanty, H. Zeng, A. Priimagi, I. Aprahamian, *J. Am. Chem. Soc.* **2021**, *143*, 16348–16353.
- [32] S. Yang, D. Larsen, M. Pellegrini, S. Meier, D. F. Mierke, S. R. Beeren, I. Aprahamian, *Chem.* **2021**, *7*, 2190–2200.
- [33] M. N. Chaur, D. Collado, J.-M. Lehn, *Chem. Eur. J.* **2011**, *17*, 248–258.
- [34] D. J. van Dijken, P. Kovaříček, S. P. Ihrig, S. Hecht, *J. Am. Chem. Soc.* **2015**, *137*, 14982–14991.
- [35] B. Mravec, J. Filo, K. Csicsai, V. Garaj, M. Kemka, A. Marini, M. Mantero, A. Bianco, M. Cigáň, *Phys. Chem. Chem. Phys.* **2019**, *21*, 24749–24757.
- [36] B. Mravec, Š. Budzák, M. Medved, L. F. Pašteka, C. Slavov, T. Saßmannshausen, J. Wachtveitl, J. Kožíček, L. Hegedüsová, J. Filo, M. Cigáň, *J. Org. Chem.* **2021**, *86*, 11633–11646.
- [37] B. Shao, I. Aprahamian, *ChemistryOpen* **2020**, *9*, 191–194.
- [38] N. Mardirossian, M. Head-Gordon, *Mol. Phys.* **2017**, *115*, 2315–2372.
- [39] K. Spiekermann, L. Pattanaik, W. H. Green, *Sci. Data* **2022**, *9*, 417.
- [40] T. Le Bahers, C. Adamo, I. Ciofini, *J. Chem. Theory Comput.* **2011**, *7*, 2498–2506.
- [41] D. Jacquemin, T. L. Bahers, C. Adamo, I. Ciofini, *Phys. Chem. Chem. Phys.* **2012**, *14*, 5383–5388.
- [42] B. Mravec, A. Marini, M. Tommasini, J. Filo, M. Cigáň, M. Mantero, S. Tosi, M. Canepa, A. Bianco, *ChemPhysChem* **2021**, *22*, 533–541.
- [43] T. Petrenko, F. Neese, *J. Chem. Phys.* **2007**, *127*, 164319.

- [44] F. Neese, *ORCA, an ab initio, density functional and semiempirical SCF-MO package, version 2.9*.
- [45] C. Slavov, H. Hartmann, J. Wachtveitl, *Anal. Chem.* **2015**, *87*, 2328–2336.
- [46] C. Slavov, C. Boumrifak, C. A. Hammer, P. Trojanowski, X. Chen, W. J. Lees, J. Wachtveitl, M. Braun, *Phys. Chem. Chem. Phys.* **2016**, *18*, 10289–10296.
- [47] S. Lee, M. Filatov, S. Lee, C. H. Choi, *J. Chem. Phys.* **2018**, *149*, 104101.
- [48] G. M. J. Barca, C. Bertoni, L. Carrington, D. Datta, N. De Silva, J. E. Deustua, D. G. Fedorov, J. R. Gour, A. O. Gunina, E. Guidez, T. Harville, S. Irle, J. Ivanic, K. Kowalski, S. S. Leang, H. Li, W. Li, J. J. Lutz, I. Magoulas, J. Mato, V. Mironov, H. Nakata, B. Q. Pham, P. Piecuch, D. Poole, S. R. Pruitt, A. P. Rendell, L. B. Roskop, K. Ruedenberg, T. Sattasathuchana, M. W. Schmidt, J. Shen, L. Slipchenko, M. Sosonkina, V. Sundriyal, A. Tiwari, J. L. Galvez Vallejo, B. Westheimer, M. Wloch, P. Xu, F. Zahariev, M. S. Gordon, *J. Chem. Phys.* **2020**, *152*, 154102.
- [49] A. Gáplovský, Š. Toma, J. Donovalová, *J. Photochem. Photobiol., A* **2007**, *191*, 162–166.
- [50] M. J. Frisch, G. W. Trucks, H. B. Schlegel, G. E. Scuseria, M. A. Robb, J. R. Cheeseman, G. Scalmani, V. Barone, G. A. Petersson, H. Nakatsuji, X. Li, M. Caricato, A. V. Marenich, J. Bloino, B. G. Janesko, R. Gomperts, B. Mennucci, H. P. Hratchian, J. V. Ortiz, A. F. Izmaylov, J. L. Sonnenberg, D. Williams-Young, F. Ding, F. Lipparini, F. Egidi, J. Goings, B. Peng, A. Petrone, T. Henderson, D. Ranasinghe, V. G. Zakrzewski, J. Gao, N. Rega, G. Zheng, W. Liang, M. Hada, M. Ehara, K. Toyota, R. Fukuda, J. Hasegawa, M. Ishida, T. Nakajima, Y. Honda, O. Kitao, H. Nakai, T. Vreven, K. Throssell, J. A. Montgomery, Jr., J. E. Peralta, F. Ogliaro, M. J. Bearpark, J. J. Heyd, E. N. Brothers, K. N. Kudin, V. N. Staroverov, T. A. Keith, R. Kobayashi, J. Normand, K. Raghavachari, A. P. Rendell, J. C. Burant, S. S. Iyengar, J. Tomasi, M. Cossi, J. M. Millam, M. Klene, C. Adamo, R. Cammi, J. W. Ochterski, R. L. Martin, K. Morokuma, O. Farkas, J. B. Foresman, D. J. Fox, *Gaussian ~16 Revision C.01*, **2016**, Gaussian Inc. Wallingford CT.
- [51] F. Weigend, *Phys. Chem. Chem. Phys.* **2006**, *8*, 1057–1065.
- [52] T. Yanai, D. Tew, N. Handy, *Chem. Phys. Lett.* **2004**, *393*, 51–57.
- [53] Y. Zhao, D. G. Truhlar, *Theor. Chem. Acc.* **2008**, *120*, 215–241.
- [54] H. S. Yu, X. He, S. L. Li, D. G. Truhlar, *Chem. Sci.* **2016**, *7*, 5032–5051.
- [55] S. Miertuš, E. Scrocco, J. Tomasi, *Chem. Phys.* **1981**, *55*, 117–129.
- [56] J. Tomasi, B. Mennucci, R. Cammi, *Chem. Rev.* **2005**, *105*, 2999–3094.
- [57] M. Cossi, V. Barone, *J. Chem. Phys.* **2001**, *115*, 4708–4717.
- [58] R. Cammi, B. Mennucci, *J. Chem. Phys.* **1999**, *110*, 9877–9886.
- [59] M. Caricato, B. Mennucci, J. Tomasi, F. Ingrosso, R. Cammi, S. Corni, G. Scalmani, *J. Chem. Phys.* **2006**, *124*, 124520.
- [60] Y.-P. Li, J. Gomes, S. Mallikarjun Sharada, A. T. Bell, M. Head-Gordon, *J. Phys. Chem. C* **2015**, *119*, 1840–1850.
- [61] R. F. Ribeiro, A. V. Marenich, C. J. Cramer, D. G. Truhlar, *J. Phys. Chem. B* **2011**, *115*, 14556–14562.
- [62] G. Luchini, J. Alegre-Requena, I. Funes-Ardoiz, R. Paton, *F1000Research* **2020**, *9*.
- [63] M. Drobizhev, N. S. Makarov, S. E. Tillo, T. E. Hughes, A. Rebane, *J. Phys. Chem. B* **2012**, *116*, 1736–1744.
- [64] S. Maeda, K. Ohno, K. Morokuma, *J. Chem. Theory Comput.* **2010**, *6*, 1538–1545.

Manuscript received: October 24, 2023

Accepted manuscript online: November 13, 2023

Version of record online: January 11, 2024